Contribution from the Department of Chemistry, University of Florence, Florence, Italy, and Laboratoire de Chimie (UA CNRS 1194), Department de Recherche Fondamentale, Centre d'Etudes Nucleaires, Grenoble, France

Structure and Magnetic Properties of Ferrimagnetic Chains Formed by Manganese(II) and Nitronyl Nitroxides

Andrea Caneschi,[1a] Dante Gatteschi,*[1a] Paul Rey,*[1b] and Roberta Sessoli[1a]

Received October 20, 1987

Four ferrimagnetic chains formed by manganese hexafluoroacetylacetonate and different nitronyl nitroxide radicals 2-R-4,4,5,5-tetramethyl-4,5-dihydro-1*H*-imidazolyl-1-oxy 3-oxide (with R = isopropyl, ethyl, methyl, and phenyl) were synthesized. The magnetic susceptibility measurements in the range 6-300 K show a divergence at low temperature that is compatible with an infinite array structure. The intrachain interaction is antiferromagnetic and estimated by a numerical fit to be in the range 200-330 cm^{-1}. The monodimensionality is confirmed by the X-ray structure of $Mn(hfac)_2NIT$-*i*-Pr, which crystallizes in the monoclinic $P2_1/c$ space group with $a = 20.135$ (1) Å, $b = 9.43$ (1) Å, $c = 15.475$ (1) Å, $\beta = 110.74$ (2)°, and $Z = 4$. EPR spectra are consistent with the magnetic data and show a behavior typical of low-dimensional materials. The line width in single-crystal spectra of $Mn(hfac)_2NIT$-*i*-Pr has an angular dependence of the type $(3\cos^2\theta - 1)^{4/3}$, while the line shape is intermediate between Lorentzian and Gaussian, showing that the exchange narrowing regime is not attained.

Introduction

Ferrimagnetic chains are one-dimensional systems in which two different spins are antiferromagnetically coupled. By different we mean either spins of a different nature, like those provided by for instance manganese(II) and copper (II) ions, or spins otherwise identical but differently oriented along the chain. Examples of both types have been reported in the literature.[2-15]

The magnetic behavior of ferrimagnetic chains is determined by the fact that the antiferromagnetic interaction cannot cancel the alternating magnetic moments. At high temperature, when the spins are uncorrelated, the χT product corresponds to the weighted average of the moments. At intermediate temperature the χT value decreases because the interaction tends to align the spins antiparallel and the states with the highest spin multiplicity are depopulated, but when the temperature is decreased further, χT increases as a consequence of the fact that short-range order keeps the uncompensated moments parallel to each other. Eventually a phase transition to three-dimensional order can occur at low temperature.

The design of magnetic materials is one of the most stimulating challenges for chemists, and in the last few years, many new novel examples of one dimensional systems have been obtained. From the chemical point of view a convenient strategy in order to synthesize alternating-spin ferrimagnetic chains consists in designing ligands capable of binding to two different metal ions with different donor atoms. In this way a few compounds, in which two different metal ions alternate regularly along one direction, have been obtained and their magnetic properties have been studied.[2-5,12,13] Very interesting behaviors have been observed both in the paramagnetic and in the ordered phase, but the reported exchange coupling constants, J, have not exceeded so far[13] 85 cm^{-1} (the Hamiltonian is written in the form $H = JS_1 \cdot S_2$).

We have now developed an alternative strategy that consists of bringing into interaction metal ions and stable organic radicals which can act as ligands.[16-18] The peculiarity of these ligands is that the unpaired electron may be described as ligand centered upon coordination. In this way we hoped to obtain substantially larger couplings between the different spins, yielding larger short-range-order effects in the paramagnetic phase and possibly higher temperatures of transition to three-dimensional order. We have obtained the most promising results with nitronyl nitroxides, stable radicals of formula

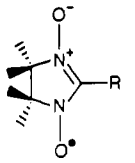

NITR = 2-R-4,4,5,5-tetramethyl-4,5-dihydro-1*H*-imidazolyl-1-oxy 3-oxide

These radicals can easily bind to two different metal atoms with their two equivalent oxygen atoms. In particular we have obtained ferromagnetic chains with copper[19] and complex chains of diamonds of four spins with nickel and cobalt.[20] We report here the magnetic properties of a series of ferrimagnetic chains of general formula $Mn(hfac)_2NITR$, where R = isopropyl, *i*-Pr, (I); ethyl, Et, (II); methyl, Me, (III); and phenyl, Ph, (IV). We also report here the X-ray crystal structure of I.

Experimental Section

Synthesis of the Complexes. $Mn(hfac)_2 \cdot 2H_2O$ was prepared according to the literature method.[21] NITR radicals (R = isopropyl, ethyl, methyl, phenyl) were prepared as previously described.[22-24] $Mn(hfac)_2NITPh$

(1) (a) University of Florence. (b) Centre d'Etudes Nucleaires.
(2) Landee, C. P. In *Organic and Inorganic Low Dimensional Crystalline Materials*; Delhaes, P., Drillon, M. Eds.; NATO ASI Series; Plenum: New York, 1987.
(3) Gleizes, A.; Verdaguer, M. *J. Am. Chem. Soc.* **1981**, *103*, 7373.
(4) Gleizes, A.; Verdaguer, M. *J. am. Chem. Soc.* **1984**, *106*, 3727.
(5) Verdaguer, M.; Gleizes, A.; Renard, J. P.; Seiden, J. *Phys. Rev. B: Condens. Matter* **1984**, *29*, 5144.
(6) Verdaguer, M.; Julve, M.; Michalowicz, A.; Kahn, O. *Inorg. Chem.* **1983**, *22*, 2624.
(7) Beltran, D.; Escriva, E.; Drillon M. *J. Chem. Soc., Faraday Trans.* **1982**, *78*, 1773.
(8) Drillon, M.; Coronado, E.; Beltran, D.; Curely, J.; Georges, R.; Nugteren, P. R.; de Jongh, L. J.; Genicon, J. L. *J. Magn. Magn. Mater.* **1986**, *54-57*, 1507.
(9) Drillon, M.; Coronado, E.; Beltran, D.; Georges, R. *Chem. Phys.* **1983**, *79*, 449.
(10) Georges, R.; Curély, J.; Drillon, M. *J. Appl. Phys.* **1985**, *58*, 914.
(11) Coronado, E.; Drillon, M.; Fuertes, A.; Beltran, D.; Mosset, A.; Galy, J. *J. Am. Chem. Soc.* **1986**, *108*, 900.
(12) Pei, Y.; Kahn, O.; Sletten, J. *J. Am. Chem. Soc.* **1986**, *108*, 3143.
(13) Pei, Y.; Verdaguer, M.; Kahn, O.; Sletten, J.; Renard, J. P. *Inorg. Chem.* **1987**, *26*, 138.
(14) Pei, Y.; Verdaguer, M.; Kahn, O.; Sletten, J.; Renard, J. P. *J. Am. Chem. Soc.* **1986**, *108*, 7428.
(15) Landee, C. P.; Djili, A.; Willet, R. D.; Place, H. In *Organic and Inorganic Low Dimensional Crystalline Materials*; Delhaes, P., Drillon, M. Eds.; NATO ASI Series; Plenum: New York, 1987.
(16) Benelli, C.; Caneschi, A.; Gatteschi, D.; Laugier, J.; Rey, P. In *Organic and Inorganic Low Dimensional Crystalline Materials*; Delhaes, P., Drillon, M. Eds.; NATO ASI Series; Plenum: New York, 1987.
(17) Caneschi, A.; Gatteschi, D.; Laugier, J.; Rey, P.; Sessoli, R.; Zanchini, C. In *Organic and Inorganic Low Dimensional Crystalline Materials*; Delhaes, P. and Drillon, M. Eds.; NATO ASI Series; Plenum: New York, 1987.
(18) Benelli, C.; Caneschi, A.; Gatteschi, D.; Laugier, J.; Rey, P. In *Organic and Inorganic Low Dimensional Crystalline Materials*; Delhaes, P. Drillon, M. Eds., NATO ASI Series; Plenum: New York, 1987.
(19) Caneschi, A.; Gatteschi, D.; Laugier, J.; Rey, P. *J. Am. Chem.* Soc. **1987**, *109*, 2191.
(20) Caneschi, A.; Gatteschi, D.; Laugier, J.; Rey, P.; Sessoli, R., submitted for publication.
(21) Cotton, F. A.; Holm, R. H. *J. Am. Chem. Soc.* **1960**, *86*, 2979.
(22) Lamchen, M.; Wittag, T. W. *J. Chem. Soc.* **1966**, 2300.

0020-1669/88/1327-1756$01.50/0

Table I. Crystallographic Data and Experimental Parameters for $Mn(hfac)_2NIT$-*i*-Pr

formula	$C_{20}H_{21}MnH_2O_6F_{12}$
mol wt	668.3
cryst syst	monoclinic
space group	$P2_1/c$
cell params	a = 20.135 (1) Å, b = 9.430 (1) Å, c = 15.475 (1) Å, β = 110.74 (2)°, V = 2747.9 Å^3, Z = 4
density	1.615 g/cm^3
linear abs	0.54 mm^{-1}
cryst size	0.50 × 0.125 × 0.100 mm
temp	20 °C
radiation	wavelength: 0.7107 Å (Mo Kα)
	monochromator: graphite
scan	mode: ω–2θ
	range: $2.5 \le \theta \le 22.5°$
	speed: 0.03°/s
test reflcn	3 reflcns every 120 min
measd reflcn	$-19 \le h \le 17$, $0 \le k \le 9$, $0 \le l \le 16$
	tot. no.: 4002
	$F \ge 6\sigma(F)$: 1162
refinement	R = 0.054
	R_w = 0.051

was obtained by suspending 1 mmol of $Mn(hfac)_2$-$2H_2O$ in 40 mL of warm *n*-heptane and adding a warm solution of *n*-heptane containing 0.95 mmol of NITPh. Immediately the suspension became yellow-green, and after being stirred for 2 min, it became green and was filtered; the precipitate, which is a mixture of $Mn(hfac)_2$·$2H_2O$ and of the adduct, was discarded. Small dark green crystals were recovered from the warm filtered solution.

$Mn(hfac)_2NIT$-*i*-Pr was prepared by dissolving 1 mmol of $Mn(hfac)_2$·$2H_2O$ in 70 mL of boiling *n*-heptane and adding to this solution 1.05 mmol of NIT-*i*-Pr radical. The violet solution was filtered, allowed to cool down, and stored at 4 °C for 1 day. Red-violet crystals suitable for X-ray crystallographic determination were obtained. $Mn(hfac)_2NITEt$ and $Mn(hfac)_2NITMe$ were obtained in the same way as $Mn(hfac)_2NIT$-*i*-Pr: up to now we have been able to obtain $Mn(hfac)_2NITMe$ only in very thin and elongated hairlike crystals.

All the compounds analyzed satisfactorily for $Mn(hfac)_2NITR$.

$Mn(hfac)_2NITPh$: Anal. Calcd for $C_{23}F_{12}H_{19}MnN_2O_6$: C, 39.32; H, 2.71; Mn, 7.82; N, 3.99. Found: C, 39.11; H, 2.65; Mn, 7.98; N, 3.90.

$Mn(hfac)_2NIT$-*i*-Pr: Anal. Calcd for $C_{20}F_{12}H_{21}MnN_2O_6$: C, 35.93; H, 3.14; N, 4.19. Found: C, 35.77; H, 3.25; N, 4.06.

$Mn(hfac)_2NITEt$: Anal. Calcd for $C_{19}F_{12}H_{19}MnN_2O_6$: C, 34.86; H, 2.90; Mn, 8.41; N, 4.26. found: C, 34.97; H, 2.95; Mn, 8.35; N, 4.17.

$Mn(hfac)_2NITMe$: Anal. Calcd for $C_{18}F_{12}H_{17}MnN_2O_6$: C, 33.75; H, 2.66, Mn, 8.59; N, 4.37. Found: C, 33.53; H, 2.77; Mn, 8.41; N, 4.19.

X-ray Analysis. Structure Determination. Diffraction data were collected at room temperature on a Philips PW1100 automated diffractometer equipped with Mo Kα radiation and a graphite monochromator. More details are given in Table I. Accurate unit cell parameters and the orientation matrix were obtained from 25 machine-centered reflections. Data were corrected for Lorentz and polarization effects.

The systematic extintions were compatible only with the space group $P2_1/c$. The early steps of the solution of the structure were based on direct methods using the MULTAN77 package.[25] After the manganese and oxygen positions were found, the other atoms were revealed by successive Fourier difference synthesis performed by using the SHELX76 program.[26] Due to the low number of intense reflections at high angles, only the manganese atom, all the fluorine atoms, and two carbon atoms were considered anisotropic. The hydrogen atoms were introduced in idealized positions and their thermal factors estimated around 20% greater than that of the respective carbon atom. The refinement converged to R = 0.054 and R_w = 0.051.

Atomic positional parameters are listed in Table II, selected bond distances and angles are given in Table III and Table IV.

Magnetic and EPR Measurements. Magnetic susceptibilities were measured in the temperature range 300–5 K by using an SHE superconducting SQUID susceptometer at a field strength of 100 G. Data were corrected for the magnetization of the sample holder and for diamagnetic contributions estimated from Pascal constants.

Room-temperature EPR spectra were recorded with a Bruker ER200 spectrometer operating at X-band frequency. A single crystal of $Mn(hfac)_2NIT$-*i*-Pr (I) used for the EPR spectra was oriented by using the same diffractometer mentioned above and was found to have highly developed (100) and ($\bar{1}$00) faces.

Table II. Positional Parameters (×10^4) and Isotropic Thermal Factors (Å^2 × 10^3)[a]

	x	y	z	B_{eq}
Mn	7463 (1)	1155 (2)	4940 (1)	45
O1	8340 (4)	2213 (8)	5964 (5)	49 (2)
O2	8237 (4)	−509 (8)	5132 (5)	48 (2)
O_3	6557 (4)	2444 (9)	4271 (5)	52 (3)
O4	6740 (4)	−529 (8)	4370 (5)	54 (3)
O5	7861 (4)	1880 (9)	3878 (5)	56 (3)
O6	7026 (4)	3986 (9)	1030 (5)	61 (3)
N2	7328 (5)	3815 (12)	1922 (7)	50 (3)
N1	7675 (5)	2848 (11)	3253 (7)	47 (3)
C11	7365 (6)	2609 (14)	2338 (8)	37 (4)
C12	7526 (7)	5057 (14)	2518 (8)	52 (4)
C13	7947 (7)	4344 (13)	3475 (8)	49 (4)
C1	8980 (7)	1888 (14)	6193 (8)	44 (4)
C2	8887 (7)	−391 (14)	5476 (8)	45 (4)
C3	9292 (8)	715 (14)	6006 (8)	56 (4)
C4	9493 (10)	3076 (21)	6736 (13)	79 (5)
C5	9274 (9)	−1637 (19)	5251 (12)	74 (5)
C6	5910 (7)	2057 (14)	4074 (8)	45 (4)
C7	6085 (8)	−448 (14)	4212 (8)	49 (4)
C8	5655 (8)	719 (14)	4041 (8)	53 (4)
C9	5408 (10)	3286 (19)	3873 (12)	71 (5)
C10	5754 (10)	−1882 (21)	4228 (13)	77 (5)
C14	7096 (8)	1226 (17)	1890 (10)	72 (4)
C15	6401 (7)	863 (16)	1987 (9)	103
C16	7607 (8)	92 (17)	2063 (11)	122
C17	7965 (6)	6088 (15)	2201 (8)	77 (4)
C18	6839 (7)	5748 (15)	2497 (9)	84 (5)
C19	7773 (7)	4903 (14)	4293 (8)	68 (4)
C20	8740 (6)	4262 (13)	3708 (8)	64 (4)
F1	10138 (5)	2683 (12)	7146 (8)	150
F2	9295 (5)	3574 (13)	7386 (7)	151
F3	9498 (7)	4111 (12)	6270 (7)	172
F4	9967 (4)	−1537 (10)	5556 (6)	103
F5	9068 (4)	−1891 (11)	4360 (6)	122
F6	9137 (5)	−2816 (10)	5627 (7)	115
F7	4737 (4)	2927 (10)	3588 (7)	127
F8	5472 (5)	4078 (10)	3179 (7)	126
F9	5525 (5)	4155 (11)	4556 (7)	134
F10	6053 (6)	−2577 (11)	4987 (8)	164
F11	5806 (6)	−2716 (11)	3589 (8)	152
F12	5081 (6)	−1883 (11)	4089 (9)	152

[a] Standard deviations in the last significant digit are given in parentheses. Standard deviations in the thermal factors are indicated only for isotropic atoms.

Table III. Selected Bond Lengths (A)[a]

Mn–O1	2.154 (8)	Mn–O5	2.177 (8)
Mn–O2	2.157 (8)	Mn–O6	2.164 (8)
Mn–O3	2.130 (8)	O5–N1	1.286 (10)
Mn–O4	2.124 (8)	O6–N2	1.307 (10)

[a] Standard deviations in the last significant digits are given in parentheses.

Table IV. Selected Bond Angles (deg)[a]

O1–Mn–O2	82.6 (3)	O3–Mn–O4	83.2 (3)
O1–Mn–O3	115.5 (3)	O3–Mn–O5	86.2 (3)
O1–Mn–O4	156.1 (3)	O3–Mn–O6	84.2 (3)
O1–Mn–O5	89.2 (3)	O4–Mn–O5	107.6 (3)
O1–Mn–O6	84.7 (3)	O4–Mn–O6	82.5 (3)
O2–Mn–O3	159.1 (3)	O5–Mn–O6	165.1 (3)
O2–Mn–O4	82.4 (3)	Mn–O5–N1	134.8 (7)
O2–Mn–O5	83.9 (3)	Mn–O6–N2	130.4 (7)
O2–Mn–O6	108.8 (3)		

[a] Standard deviations in the last significant digits are given in parentheses.

(23) Ullman, E. F.; Call, L.; Osiecky, J. H. *J. Org. Chem.* **1970**, *35*, 3623.
(24) Ullman, E. F.; Osiecky, J. H.; Boocock, D. G. B.; Darcy, R. *J. Am. Chem. Soc.* **1972**, *94*, 7049.
(25) Main, P.; Woolfson, M. M.; Germain, G. "MULTAN 77 Direct Methods Program".
(26) Sheldrick, G. "SHELX 76 System of Computing Programs"; University of Cambridge: Cambridge, England, 1976.

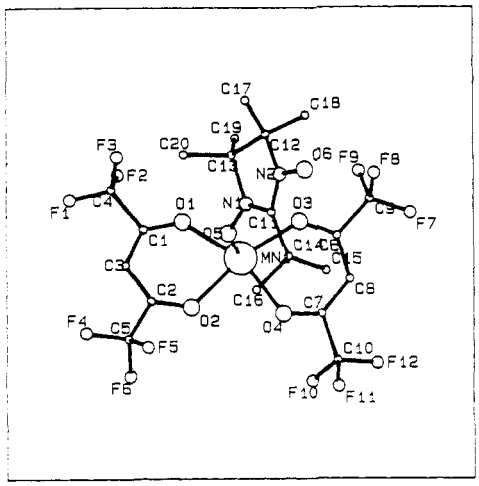

Figure 1. Asymmetric unit of $Mn(hfac)_2NIT$-*i*-Pr.

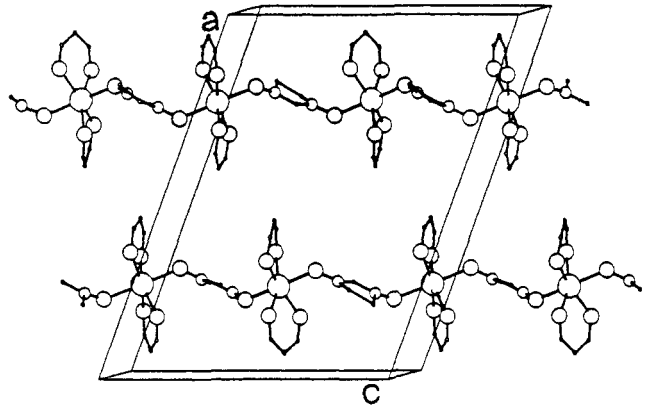

Figure 2. View of the unit cell of $Mn(hfac)_2NIT$-*i*-Pr. The methyl and trifluoromethyl groups have been omitted for the sake of clarity.

Results

Crystal Structure. $Mn(hfac)_2NIT$-*i*-Pr crystallizes in the monoclinic system, space group $P2_1/c$. The structure consists of chains of $Mn(hfac)_2$ units bridged by NIT-*i*-Pr radicals. The asymmetric unit is comprised of a $Mn(hfac)_2NIT$-*i*-Pr group, shown in Figure 1. The unit cell is shown in Figure 2, where two equivalent chains oriented along the *c* axis are clearly visible.

Each manganese(II) ion is hexacoordinated by four oxygen atoms of two different hfac molecules and by two oxygen atoms of two different NIT-*i*-Pr radicals. The average Mn–O distance relative to hfac ligands compares well with that observed in other radical adducts while the Mn–O distances relative to the NIT-*i*-Pr molecule is the largest so far observed in manganese–nitroxide complexes.[27-29] The bond angles within the coordination octahedron are severely distorted. The two average planes defined by the hfac skeleton form an angle of 27° and the group Mn–O1–O2–O3–O4 is far from planar with O1 and O4 0.25 and 0.32 Å above the average plane and with O2 and O3 0.30 and 0.25 Å below. The two radical oxygen atoms are axially coordinated, but the Mn–O directions form an angle of 164.7°. The origin of this distortion is probably to release steric hindrance between hfac and the nitroxides.

The bond distances and angles within the radical are fairly normal. The N–O distances compare well with those previously reported for coordinated NITR radicals.[19,28-31] They are slightly different from each other, and so are also the Mn–O distances. The Mn–O–N angles are 134.8 (7)° and 130.4 (7)°, comparing well with the values reported in other NITR derivatives[17,18] and significantly smaller than those observed in nitroxide derivatives.[19,20] The five-membered ring is fairly planar with the two carbon atoms carrying the methyl groups 0.11 Å above and below the average plane.

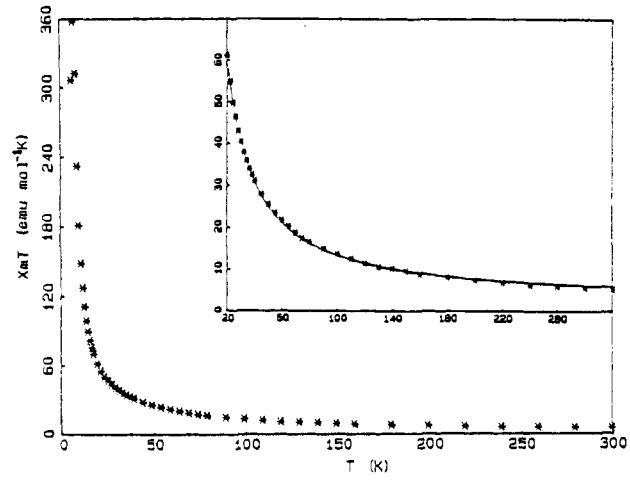

Figure 3. χT vs temperature for I. In the inset the solid line is calculated as described in the text.

Magnetic Properties. The temperature dependence of χT for I is shown in Figure 3. The behaviors of II–IV are very similar and are reported as supplementary material (Figures S1–S3). At room temperature the value of χT for the series is in the range 4.3–5.3 emu mol^{-1} K, and it increases sharply with decreasing temperature. Below 8 K, a sharp decrease in χT is observed, presumably due to saturation effects. The highest observed χT values are in the range 250–360 emu $mol^{-1}K$, a clear indication of an infinite array of spins in agreement with the structure of $Mn(hfac)_2NIT$-*i*-Pr. The magnetic properties of I–IV are plotted in Figure 4 in a log χ vs log T form, in order to have an indication of the rate of divergence of the susceptibility and of possible phase transitions. The behavior of the four compounds is again fairly similar, with a quasi-linear high-temperature region, and a low-temperature region where the rate initially increases and then levels off. The linear region has a slope of about 1.85 for all the compounds, and deviation from linearity is observed in the range 7–10 K.

EPR Spectra. Polycrystalline powder EPR spectra of the four compounds are rather similar to each other with a single line centered at $g = 2$.

The line width varies in the series as follows: $\Delta H_{pp} = 75$ G for I, 105 G for II, 140 G for III, and 160 G for IV.

More information is obtained from single-crystal spectra of compound I. In every orientation only a single line is observed at $g = 2$. The line width depends heavily on the angle formed by the static field and the *c* direction, the direction of the chain. In the plane perpendicular to the *c* axis the spectra are almost isotropic. The dependence of the line width on the orientation is reported in Figure 5 in the form ΔH_{pp} vs. θ, where θ is the angle between the static field and *c*. The line width reaches a maximum (430 G) parallel to the chain, a deep minimum (68 G) is observed at the magic angle, and another relative maximum (210 G) is observed when the field is perpendicular to the chain direction. No half-field transitions are observed.

The line shape was analyzed with the standard procedure.[32,33] At $\theta = 54°$ the line is Lorentzian as shown in Figure 6, while it

(27) Dickman, M. H.; Porter, L. C.; Doedens, R. J. *Inorg. Chem.* **1986**, *25*, 2595.
(28) Caneschi, A.; Gatteschi, D.; Pardi, L.; Rey, P.; Zanchini, C., submitted for publication.
(29) Caneschi, A.; Gatteschi, D.; Laugier, J.; Rey, P.; Sessoli, R.; Zanchini, C., submitted for publication.
(30) Caneschi, A.; Gatteschi, D.; Grand, A.; Laugier, J.; Pardi, L.; Rey, P. *Inorg. Chem.*, in press.
(31) Benelli, C.; Caneschi, A.; Gatteschi, D.; Laugier, J.; Rey, P. *Angew. Chem.* **1987**, *99*, 958.
(32) Bartkowski, R. R.; Morosin, B. *Phys. Rev. B: Solid State* **1972**, *6*, 4209.
(33) Bartkowski, R. R.; Hennessy, M. J.; Morosin, B.; Richards, P. M. *Solid State Commun.* **1972**, *11*, 405.
(34) Seiden, J. *J. Phys., Lett.* **1983**, *44*, L947.

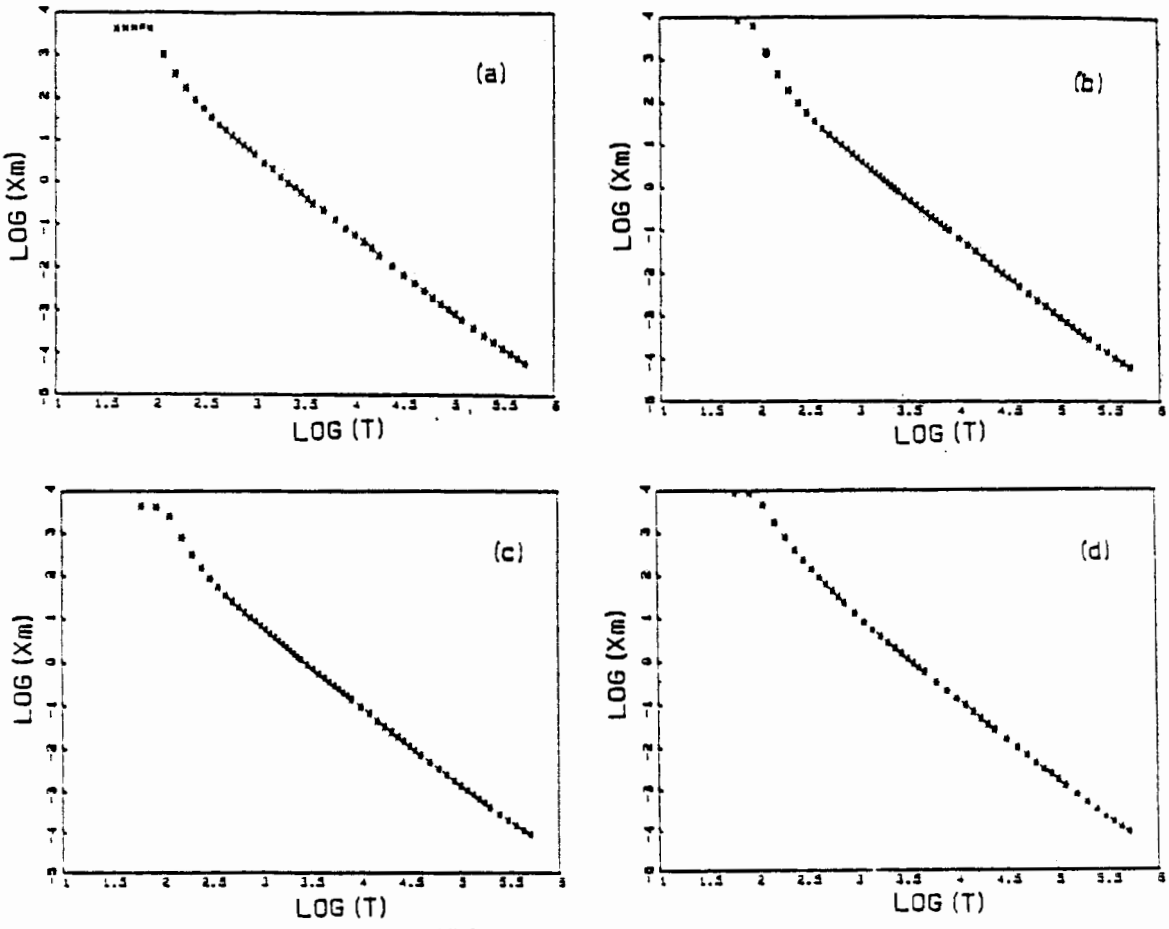

Figure 4. Plots of log χ vs log T: (a) I; (b) II; (c) III; (d) IV.

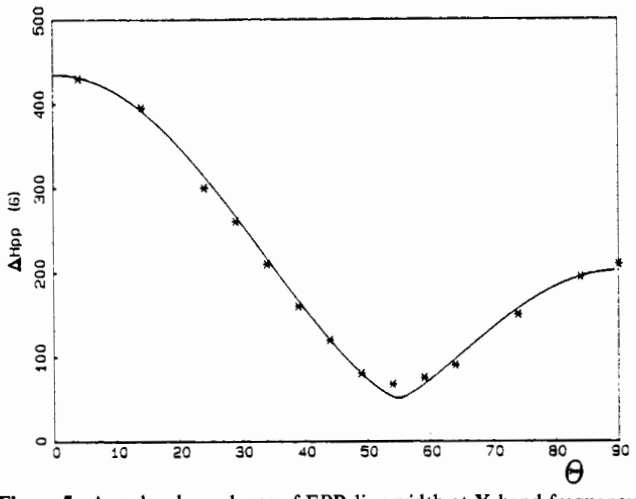

Figure 5. Angular dependence of EPR line width at X-band frequency and room temperature for I. The solid line is the plot of $a + b(3\cos^2\theta - 1)^{4/3}$ with $a = 49.9$ and $b = 152.8$ G.

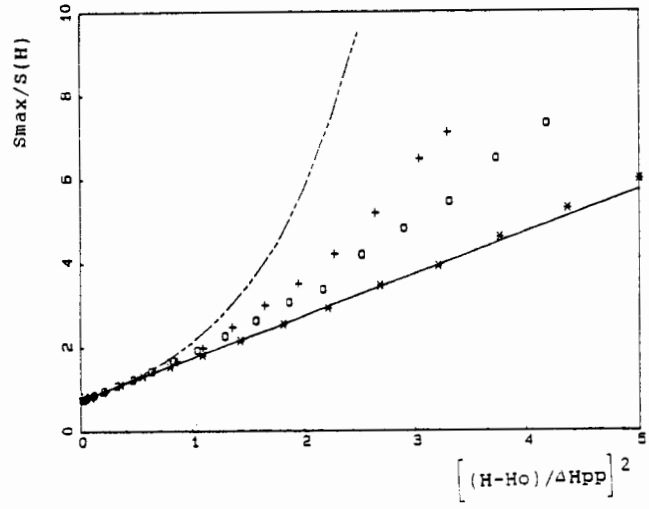

Figure 6. Line-shape analysis for I at angular setting of the field: (+) $\theta = 0°$; (○) $\theta = 90°$; (*) $\theta = 54°$. The solid line corresponds to the theoretical curve for a Lorentzian line while the broken line corresponds to the Gaussian line. $S(H) = (Y(H)/(H - H_0))^{1/2}$, where Y is the amplitude of the derivative of the absorption.

is intermediate between Gaussian and Lorentzian for $\theta = 0°$ and 90°.

Discussion

The similarity of the magnetic properties of I–IV clearly indicates that all of them must have the same chain structure seen in $Mn(hfac)_2NIT\text{-}i\text{-}Pr$. In fact the divergence of χ observed at low temperature is only compatible with an infinite array. In principle this might be due either to ferro- or ferrimagnetic chains. The magnetic behavior of the latter class has been studied in some detail,[5,9,10,33] and it has been found that the χT vs T curve has a high-temperature limit of 4.75 emu mol^{-1} K, assuming $g = 2$, decreases slightly on decreasing temperature to reach a minimum at $T = 2.27J/k$ corresponding to $\chi T \sim 4$ emu mol^{-1} K, and then diverges at lower temperatures. The behavior of ferromagnetic chains composed of $S = {}^1/_2$ and $S = {}^5/_2$ pairs has not been studied so far, but the qualitative behavior may easily be anticipated: at high temperature χT has the same limit as in the ferrimagnetic case and increases steadily with decreasing temperature.

The χT vs T curves of I–IV do not show any minimum. Two alternative explanations can be suggested for this: (i) the coupling is ferromagnetic; (ii) the coupling is antiferromagnetic, and J is larger than 92 cm^{-1}, thus yielding a minimum above 300 K. We choose the latter possibility for the following reasons: the exchange interaction between manganese(II) and nitroxide radicals has been

Table V. Best Fit and EPR Line Width for $Mn(hfac)_2NITR$

R	J,[a] cm^{-1}	ΔH_{pp},[b] G
i-Pr	329.8	75
Et	259.5	105
Me	216.7	140
Ph	208.2	160

[a] The fit is performed by using expression 1. [b] The line width is evaluated from the polycrystalline EPR spectra.

found to be antiferromagnetic in all the cases reported so far[27,28] and to have J values larger than 150 cm^{-1}. In particular it has been found to be antiferromagnetic in an oligonuclear compound with a ring structure.[29] Further the room-temperature values of χT for III and IV, which are lower than the high-temperature limit of 4.75 emu $mol^{-1}K$, are consistent with ferri- but not with ferromagnetic chains.

For a quantitative analysis of the thermodynamic properties of chains of alternate $S = {}^1/_2$ and $S = {}^5/_2$ spins, the simplest available model for monodimensional systems of Heisenberg type uses classic spins,[9] according to the original suggestion of Fischer.[35] This model is expected to be more accurate the higher the spin value. Therefore its application to the present case is hampered by the $S = {}^1/_2$ of the radicals. In order to overcome this difficulty, two alternative models have been recently suggested, which take into account the quantum nature of the $S = {}^1/_2$ spins. One of the two,[5] which uses a numerical approach, cannot be used for temperatures lower than $0.25J$, where J is in Kelvin; therefore, it is doubtful that it can be used in this case where, according to our qualitative analysis above, J/k is larger than 132 K. The other model,[34] introducing the quantum nature of $S = {}^1/_2$ in the two-spins correlation function, yields the following expression for the susceptibility:

$$\chi = \frac{1}{3}N\mu_B{}^2\beta\left[g^2S^2\left(\frac{S+1}{S} + 2\frac{-\delta}{1-\delta}\right) - 4GgSs\frac{\tau}{1-\tau} + g^2\left(s(s+1) + 2s^2\frac{\tau^2}{1-\delta}\right)\right] \quad (1)$$

where

$$\tau = \frac{(2\alpha^{-1} + 4\alpha^{-3})\cosh\alpha - 4\alpha^{-2}\sinh\alpha - 4\alpha^{-3}}{2(\alpha^{-1}\sinh\alpha - \alpha^{-2}\cosh\alpha + \alpha^{-2})}$$

$$\delta = \frac{(\alpha^{-1} + 12\alpha^{-3})\sinh\alpha - (5\alpha^{-2} + 12\alpha^{-4})\cosh\alpha - \alpha^{-2} + 12\alpha^{-4}}{2(\alpha^{-1}\sinh\alpha - \alpha^{-2}\cosh\alpha + \alpha^{-2})}$$

$$\alpha = \frac{JS}{kT}$$

The capital letters G and S refer to the spin of ${}^5/_2$.

Both of these models have been previously used for manganese–copper chains. The classic spin and the classic–quantic spins models do not have limitations on the sign of J and can be used for both ferro- and antiferromagnetic interaction.

In Table V we report the best fit values of J, obtained through a least-squares procedure using a g value of 2 for both manganese and radical spins. All of the calculated values are positive, confirming the ferrimagnetic nature of the chains. The order is NITPh ≤ NITMe ≤ NITEt ≤ NIT-*i*-Pr. The values calculated by using the Fischer model are smaller, but they follow the same trend. These values compare well with those reported for mononuclear manganese–radical complexes,[27-29] but a quantitative comparison appears to be out of order here because of the substantial differences in the models of calculation of the coupling constants. More significant is the comparison with copper–manganese chains,[3-5,33] where the same models we use here give much smaller values of the coupling constants, showing that indeed stronger interaction can be obtained with manganese and radicals compared with bimetallic chains. The divergence calculated with (1) depends on T^{-2}, which compare satisfactorily with the experimental value $T^{-1.85}$.

The lowest temperature we included in the above fit is 20 K, because below this limit saturation effects and probably deviations due to a phase transition to three-dimensional order complicate the observed magnetic behavior. We are currently attempting to characterize the magnetic properties of I–IV below 20 K, but the ferromagnetic nature of the transition can be anticipated by the increase of the divergence rate. For a bimetallic copper–manganese chain,[5] a decrease of the slope is observed, indicating the presence of transition to an antiferromagnetically ordered phase.

The values of the critical temperatures, evaluated from the log χ – log T plot, are in the range of 7 K. Therefore, although the intrachain interaction is substantially stronger than in copper–manganese chains, the transition to three-dimensional order occurs essentially in the same range of temperature, due to the fact that the interchain interaction must be fairly weak in the $Mn(hfac)_2NITR$ compounds. The largest χT values observed correspond to segments of about 150 correlated Mn–NITR pairs.

EPR spectra of the four compounds agree well with the linear-chain structure and with the observed magnetic properties. The line widths of the polycrystalline powder spectra are in the reverse order of the calculated J values. Since ΔH_{pp} is expected to be inversely proportional to J in exchange-narrowed compounds[36] and to $J^{1/3}$ in one-dimensional materials,[37] the two sets of data, EPR and magnetic fit, appear to be consistent.

The single-crystal spectra of I are typical of one-dimensional materials with large spin-diffusion effects. The half-width at half-height of monodimensional systems is given by[38]

$$\Delta H_{1/2} \cong 1.744\frac{M_2{}^{2/3}}{(J/h)^{1/3}} \quad (2)$$

where M_2 is the second moment and J is the intrachain coupling constant. The second moment in $Mn(hfac)_2NIT$-*i*-Pr may have in principle two main contributions originated by dipolar interaction and single-ion zero-field splitting. The dipolar interaction cannot be easily calculated in these compounds where the unpaired spin density on the radical is highly delocalized and the distance from the metal ion is not large compared to the charge separation.

For an ideal linear chain with uniform dipolar **D** tensors the secular part of the second moment can be calculated from

$$M_2 = \frac{3S_R(S_R+1)S_M(S_M+1)}{S_R(S_R+1) + S_M(S_M+1)}(D/3)^2(3\cos^2\theta - 1)^2 \quad (3)$$

The angular dependence of the line width becomes of the type $(3\cos^2\theta - 1)^{4/3}$, in good agreement with the observed behavior as can be seen in Figure 5. For $\theta = 0°$, where the secular terms are dominant, we have found that in order to reproduce the experimental value $\Delta H_{pp} = 430$ G the D parameter must be ≅0.2 cm^{-1}, a value that agrees well with the values suggested by the EPR spectra of other manganese–nitroxide complexes.[39] $Mn(hfac)_2NIT$-*i*-Pr has a zigzag structure, and some differences from the typical one-dimensional behavior may be expected. If we try to evaluate the second moment for the four dipolar **D** tensors, which have different principal axes in the unit cell, we still predict an angular dependence that is very similar to $(3\cos^2\theta - 1)^{4/3}$.

The line shape, which is intermediate between Gaussian and Lorentzian, except at the magic angle where it is Lorentzian, as can be seen in Figure 6, is another strong indication of the one-dimensional nature of $Mn(hfac)_2NIT$-*i*-Pr.[37] In fact interchain

(35) Fischer, M. E. *Am. J. Phys.* **1964**, *32*, 343.
(36) Abragam, A.; Bleaney, B. *Electron Paramagnetic Resonance of Transition Ions*; Oxford University Press: London, 1970.
(37) Richards, P. M. In *Local Properties at Phase Transition*; Editrice Compositori: Bologna, Italy, 1975.
(38) Hennessy, M. J.; McElwee, C. D.; Richards, P. M. *Phys. Rev. B: Solid State* **1973**, *7*, 930.
(39) Benelli C.; Gatteschi, D.; Zanchini, C.; Doedens, R. J.; Dickman, M. H.; Porter, L. C. *Inorg. Chem.* **1986**, *25*, 3453.

interactions are particularly effective in destroying the typical one-dimensional line shape, corresponding to the Fourier transform of $\Phi = \exp(-\gamma t)^{3/2}$, restoring the Lorentzian line shape of exchange-narrowed systems.[38]

On a quantitative basis this is monitored by a characteristic time t_0, at which interchain flips become important. The order of magnitude estimating for one-dimensional spin systems is

$$t_0^{-1} \cong \frac{J'}{h}(J'/J)^{1/3}$$

Numerical calculations[38] showed that notable deviations from Lorentzian line shape can be observed when $J'/J \leq 10^{-2}$. This may be considered to be a very high upper limit for the J'/J ratio, since we do not observe transitions to three-dimensional order above 10 K, suggesting that $J'/J \leq 10^{-3}$.

If we consider that every chain is surrounded by six other chains with the shortest contact of 9.43 Å, the small value of J' is not surprising. This is a desirable property if one is interested in monodimensional behavior, but it is much less appealing if the purpose is designing compounds with bulk magnetic properties. Clearly, although strong intrachain interaction can be obtained by using metal ions and radicals, it is necessary to introduce groups that can enhance interchain interactions in order to have relatively high temperature magnetic materials. Nevertheless it is certainly encouraging that the transition to three-dimensional order seems not to be of the antiferromagnetic type.

Acknowledgment. Thanks are due to the Italian Ministery of Public Education and the CNR for funding this research. The valuable help of Prof. M. Di Vaira in solving the crystal structure is gratefully acknowledged.

Registry No. $Mn(hfac)_2NITPh$, 113533-14-5; $Mn(hfac)_2NIT$-*i*-Pr, 113547-96-9; $Mn(hfac)_2NITEt$, 113533-16-7; $Mn(hfac)_2NITMe$, 113533-18-9; $Mn(hfac)_2$, 19648-86-3.

Supplementary Material Available: Tables of derived hydrogen positions (Table SII), anisotropic thermal parameters (Table SIII), complete bond distances (Table SIV), and complete bond angles (Table SV) for $Mn(hfac)_2NIT$-*i*-Pr and plots of experimental χT values vs T for II (Figure S1), III (Figure S2), and IV (Figure S3) (10 pages); a table of observed and calculated structure factors (6 pages). Ordering information is given on any current masthead page.

Contribution from the Department of Chemistry and Ames Laboratory, Iowa State University, Ames, Iowa 50011

Noninvasive Tagging of Proteins with an Inorganic Chromophore. Selectivity of Chloro(terpyridine)platinum(II) toward Amino Acids, Peptides, and Cytochromes *c*

Herb M. Brothers II and Nenad M. Kostić*

Received June 12, 1987

The complex $[Pt(trpy)Cl]^+$ exhibits unexpected selectivity toward amino acid side chains in cytochromes *c* from *Candida krusei* and bakers' yeast. Although kinetic studies with amino acids and peptides as entering ligands prove this complex to be completely selective toward thiol over imidazole, His-33 and His-39 residues (in both proteins) are labeled with greater yields than the Cys-102 residue (in the bakers' yeast protein). The binding sites are determined by peptide mapping and other methods. The $Pt(trpy)^{2+}$ tags are stable, and the protein derivatives are separated by cation-exchange chromatography. The $[Pt(trpy)His]^{2+}$ and $[Pt(trpy)Cys]^+$ chromophores are easily detected and quantitated owing to their characteristic and strong UV–vis bands. Spectroscopic and electrochemical measurements show that labeling with the new reagent does not alter the structural and redox properties of the cytochromes *c*. The unexpected outcome of the protein labeling indicates that, contrary to the common assumption, Cys-102 is not exposed at the protein surface. Modification of this residue with various organic reagents and dimerization of the protein must be accompanied by a perturbation of the conformation, which makes Cys-102 accessible to the reagent or to another molecule of the protein. These predictions from the labeling study are confirmed subsequently by the crystallographic study of the *iso*-1 cytochrome *c* from bakers' yeast. The inorganic complex $[Pt(trpy)Cl]^+$ differs from the other reagents for protein modification by its noninvasiveness, a property that may well render it useful as a probe of the protein surface.

I. Introduction

Covalent modification of amino acid side chains has proved very useful in structural, spectroscopic, and mechanistic studies of proteins.[1-3] Various spin labels, chromophores, fluorescent probes, and radioactive labels developed to date are mostly organic compounds. Except as heavy-atom scatterers in crystallographic studies,[4,5] metal complexes have not been used widely for covalent modification of proteins although their properties are well suited for this purpose.[6,7] Transition-metal complexes can serve as absorption chromophores, as paramagnetic EPR labels, as NMR probes and relaxation agents, and as electron-transfer reagents. Selectivity in binding can be controlled by the oxidation state, hardness or softness, coordination number, ancillary ligands, and charge.

Previous research in this laboratory showed that chloro(2,2′:6′,2″-terpyridine)platinum(II), $[Pt(trpy)Cl]^+$, reacts specifically with histidine (His) residues in cytochromes *c* from horse and tuna at pH 5.0.[8] The $Pt(trpy)His^{2+}$ complex, formed by

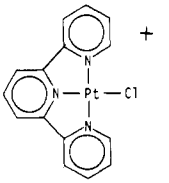

$[Pt(trpy)Cl]^+$

(1) (a) Lundblad, R. L.; Noyes, C. M. *Chemical Reagents for Protein Modification*; CRC Press: Boca Raton, FL, 1984; Vols. I and II. (b) Means, G. E.; Feeney, R. E. *Chemical Modification of Proteins*; Holden-Day: San Francisco, CA, 1971.
(2) Glazer, A. N. In *The Proteins*, 3rd ed.; Neurath, H., Ed.; Academic: New York, 1977; Vol. 2, Chapter 1 and references cited therein.
(3) Sulkowski, E. *Trends Biotechnol.* **1985**, *3*, 1.
(4) Blundell, T. L.; Johnson, L. N. *Protein Crystallography*; Academic: New York, 1976; Chapter 8.
(5) Petsko, G. A. *Methods Enzymol.* **1985**, *114*, 147.
(6) Barton, J. K. *Comments Inorg. Chem.* **1985**, *3*, 321 and references cited therein.
(7) Pullman, B., Goldblum, N., Ed. *Metal-Ligand Interaction in Organic Chemistry and Biochemistry*; D. Reidel: Boston, MA, 1977.
(8) Ratilla, E. A. M.; Brothers, H. M., II; Kostić, N. M. *J. Am. Chem. Soc.* **1987**, *109*, 4592.

0020-1669/88/1327-1761$01.50/0